JOURNAL OF GEOPHYSICAL RESEARCH, VOL. 103, NO. D3, PAGES 3399-3417, FEBRUARY 20, 1998

A global interactive chemistry and climate model: Formulation and testing

Chien Wang, Ronald G. Prinn, and Andrei Sokolov

Joint Program on the Science and Policy of Global Change, Massachusetts Institute of Technology, Cambridge

Abstract. In order to elucidate interactions between climate change and biogeochemical processes and to provide a tool for comprehensive analysis of sensitivity, uncertainty, and proposed climate change mitigation policies, we have developed a zonally averaged two-dimensional model including coupled biogeochemical and climate submodels, as a part of an integrated global system model. When driven with calculated or estimated trace gas emissions from both anthropogenic and natural sources, it is designed to simulate centennial-scale evolution of many radiatively and chemically important tracers in the atmosphere. Predicted concentrations of chemical species in the chemistry submodel are used interactively to calculate radiative forcing in the climate submodel, which, in turn, provides winds, temperatures, and other variables to the chemistry submodel. Model predictions of the surface trends of several key species are close to observations over the past 10-20 years. Predicted vertical distributions of climate-relevant species, as well as seasonal variations, are also in good agreement with observations. Runs of the model imply that if the current increasing trends of anthropogenic emissions of climate-relevant gases are continued over the next century, the chemical composition of the atmosphere would be quite different in the year 2100 than that currently observed. The differences involve not only higher concentrations of major long-lived trace gases such as CO_2, N_2O, and CH_4 but also about 20% lower concentrations of the major tropospheric oxidizer (OH free radical), and almost double the current concentrations of the short-lived air pollutants CO and NO_x.

1. Introduction

Concerns about future climate change involve not only the impact of increases of long-lived trace gases in the atmosphere on the climate (e.g., surface temperature, precipitation, and cloud coverage) but also the influence of climate change on atmospheric chemical processes and the possible effects of products of these processes, such as aerosols, on climate.

The lifetimes of chemical species in the atmosphere are affected by many processes, including atmospheric transport, chemical reactions, wet and dry deposition, exchange with the ocean or vegetation, and emissions from both human-related and natural processes. One needs to include treatment of each of these processes to address accurately the climatic effects of atmospheric chemical species and the influence of climate change on atmospheric chemistry. To address feedbacks between chemistry and climate, it is clear that a coupled numerical model including explicit descriptions of both climate dynamics and atmospheric chemistry is needed.

In recent years, models addressing both climate and chemistry with various levels of coupling between these two components have been developed [e.g., *Hauglustaine et al.*, 1994; *Taylor and Penner*, 1994; *Roelofts and Lelieveld*, 1995; *Moxim et al.*, 1996; *Levy et al.*, 1996]. However, to quantify the magnitude and uncertainty of the effects on climate of long-lived trace gases (and vice versa), a large number of long (≥100 years) transient integrations using fully coupled models with special attention to surface fluxes need to be carried out. A model would in particular have to be computationally efficient so that many runs can be made in order to understand the relative importance of various climate-chemistry feedbacks, to determine sensitivity of the results to the many critical assumptions in submodels, and (through comparison with observations) to make improvements. Constructing such a coupled model is both a theoretical and computational challenge.

Toward the goal of obtaining a better quantitation of climate-chemistry interactions and their uncertainty, we have developed a coupled global-scale modeling system including a global climate model and an atmospheric chemistry model. This system is designed to predict as functions of time, latitude and altitude the zonally averaged concentrations of the major chemically and radiatively important trace species in the atmosphere. The chemistry and climate submodels in this system are fully interactive. Specifically, the transport of chemical species is driven by dynamical variables predicted by the climate model, and the calculations of gaseous and aqueous phase reactions are based on the temperatures, radiative fluxes, and precipitation rates computed in the climate model. Predicted mixing ratios of trace species are then used, in turn, to calculate the radiative forcing in the climate model.

This paper describes the coupled model in detail, with a special focus on the chemistry component that has not yet been published. Results from a 124-year "reference" run and

Paper number 97JD03465.
0148-0227/98/97JD-03465$09.00

tests of the model using observational data are then presented. The last section provides a critique of these results and some conclusions. Further analyses focusing on the dynamics of the interactions between atmospheric chemistry and climate change are discussed by C. Wang and R. Prinn (Interactions among emissions, atmospheric chemistry, and climate change: Implications for future trends, submitted to *Journal of Geophysical Research*, 1997).

2. Model Descriptions

The climate submodel used in the coupled model is the Massachusetts Institute of Technology (MIT) two-dimensional (2-D) land-ocean-resolving (LO) statistical-dynamical model [*Sokolov and Stone*, 1995; 1997]. It is a modified version of a model developed at the Goddard Institute for Space Studies (GISS) [*Yao and Stone*, 1987; *Stone and Yao*, 1987; 1990]. The original version of the 2-D model was developed from the 3-D GISS general circulation model (GCM) of *Hansen et al.* [1983]. As a result, the model's numerics and parameterizations of physical processes, such as radiation and convection, closely parallel those of the GISS GCM. The 2-D LO model solves the primitive equations as an initial value problem. The grid used in the model consists of 24 divisions in latitude (corresponding to a resolution of 7.826°) and nine divisions in the vertical (two in the planetary boundary layer, five in the troposphere, and two in the stratosphere). The nine vertical subdivisions of the model are centered at 959, 894, 786, 634, 468, 321, 201, 103, and 27 hPa. The important feature of the 2-D LO model, from the point of view of coupling chemistry and climate dynamics, is the inclusion in its radiation code of all significant greenhouse gases, such as H_2O, CO_2, CH_4, N_2O, $CFCl_3$, CF_2Cl_2, and ozone, along with 12 types of aerosols, each as functions of latitude and time using the prescribed (O_3) or predicted (aerosol) distributions.

One special aspect of this model is that its statistical-dynamical module for predicting climate is 20 times faster than three-dimensional models with similar latitudinal and vertical resolution. While two dimensional, it resolves the ocean and land separately at each latitude and reproduces many characteristics of the current zonally averaged observed climate. The responses of this model to various climate forcings are similar to those of three-dimensional GCMs. The climate component of the 2-D LO model simulates current climate reasonable well and mimics much of the behaviors of its parent GISS GCM as well as other GCMs [*Sokolov and Stone*, 1997]. The 2-D LO model is already fully described by *Sokolov and Stone* [1995; 1997]. The focus of this paper is primarily on the chemistry submodel and on the coupling of these two submodels.

Our chemistry submodel is designed to use the same coordinate system as the climate submodel. It has 25 chemical species including CO_2, CH_4, N_2O, O_3, CO, H_2O, NO_x, HO_x, SO_2, sulfate aerosol, and chlorofluorocarbons. In its present version, the model does not include nonmethane hydrocarbon chemistry. This simplification is expected to lead to underestimation of ozone production, especially in polluted areas. Denoting zonally averaged variables with overbars and deviations from zonally averaged variables with primes, the zonally averaged mole fraction of any chemical species C, is predicted by solving the following mass conserving equation:

$$\frac{\partial \overline{\Psi}}{\partial t} = \bar{S}_{advection} + \bar{S}_{eddy} + \bar{S}_{convection} + \bar{S}_{emission} + \bar{S}_{reaction} + \bar{S}_{deposition} \quad (1)$$

where

$$\overline{\Psi} = \overline{\pi C} \quad (2)$$

$$\bar{\pi} = \bar{P}_S - \bar{P}_T \quad (3)$$

$$\bar{S}_{advection} = -\frac{\partial}{\partial \eta}\left(\frac{\overline{v\Psi}}{m}\right) - \frac{\partial}{\partial \sigma}\left(\frac{\overline{\omega\Psi}}{mn}\right) \quad (4)$$

$$m = (a \cos \eta)^{-1} \quad (5)$$

$$n = a^{-1} \quad (6)$$

$$\sigma = \frac{\bar{P} - \bar{P}_T}{\bar{P}_S - \bar{P}_T} \quad (7)$$

$$\bar{\omega} = \frac{d\sigma}{dt} \quad (8)$$

Here P_S, P, and P_T represent pressure at the surface, at an arbitrary grid point, and at the top of the atmosphere (fixed at 10 hPa); η is latitude; a is the Earth's radius; and v is the meridional wind speed. The right-hand side of equation (1) includes all the major chemical source and sink terms, as well as the advective term as described by equation (4).

The continuity equations for $CFCl_3$, CF_2Cl_2, N_2O, O_3, CO, CO_2, NO, NO_2, N_2O_5, HNO_3, CH_4, CH_2O, SO_2, and H_2SO_4 include convergence due to transport (advection, eddy diffusion, and convection), whereas the remaining very reactive atoms, free radicals, or molecules are assumed to be unaffected by transport (photochemical steady states) due to their very short lifetimes. Water vapor and air (N_2 plus O_2) densities are computed in the climate submodel. The climate submodel also provides the wind speeds, temperatures, solar radiative fluxes, and precipitation fluxes used in the chemical simulations.

2.1. Advection

The advection scheme is fourth-order and positive-definite [*Wang and Chang*, 1993; *Wang and Crutzen*, 1995], and based on a scheme suggested by *Bott* [1989a, b, 1993]. It is used in a time-splitting procedure to calculate advection along each spatial dimension in order. Then a nonoscillating scheme is used to limit the numerical errors induced by possible overestimation of fluxes during the advective calculations [*Smolarkiewicz and Grabowski*, 1990]. Finally, a mass adjustment for correcting the error induced by time splitting and non-convergence-free wind fields is used [*Kitada*, 1987].

2.2. Eddy Diffusion and Convective Transport

The parameterization developed by *Stone and Yao* [1990] for meridional eddy diffusion of water vapor and temperature in zonally averaged models has been used in this model for all transported chemical species. From *Stone and Yao* [1990], the

Table 1. Gaseous Phase Chemical Reactions Included in the Model

Number	Reaction	Reference for Rate Constants
(R1)	$O_3 + h\nu \rightarrow O(^1D) + O_2$	1
(R2)	$O(^1D) + H_2O \rightarrow 2OH$	1
(R3)	$O(^1D) + N_2 \rightarrow O + N_2$	1
(R4)	$O(^1D) + O_2 \rightarrow O + O_2$	1
(R5)	$CO + OH \rightarrow H + CO_2$	2
(R6)	$H + O_2 + M \rightarrow HO_2 + M$	2
(R7)	$HO_2 + NO \rightarrow OH + NO_2$	1
(R8)	$NO_2 + h\nu \rightarrow NO + O$	1
(R9)	$O + O_2 + M \rightarrow O_3 + M$	2
(R10)	$HO_2 + O_3 \rightarrow OH + 2O_2$	2
(R11)	$OH + O_3 \rightarrow HO_2 + O_2$	2
(R12)	$NO + O_3 \rightarrow NO_2 + O_2$	2
(R13)	$NO_2 + OH + M \rightarrow HNO_3 + M$	2
(R14)	$NO_2 + O_3 \rightarrow NO_3 + O_2$	1
(R15)	$NO_3 + NO_2 + M \rightarrow N_2O_5 + M$	2
(R16)	$HO_2 + HO_2 \rightarrow H_2O_2 + O_2$	2, 3
(R17)	$H_2O_2 + h\nu \rightarrow 2OH$	1
(R18)	$H_2O_2 + OH \rightarrow HO_2 + H_2O$	2
(R19)	$HO + HO_2 \rightarrow H_2O + O_2$	2
(R20)	$HO + HO \rightarrow H_2O + O$	2
(R21)	$HO + HO + M \rightarrow H_2O_2 + M$	2
(R22)	$CH_4 + OH \rightarrow CH_3 + H_2O$	2
(R23)	$CH_3 + O_2 + M \rightarrow CH_3O_2 + M$	2
(R24)	$CH_3O_2 + NO \rightarrow CH_3O + NO_2$	1
(R25)	$CH_3O + O_2 \rightarrow CH_2O + HO_2$	2
(R26)	$CH_3O_2 + HO_2 \rightarrow CH_3O_2H + O_2$	1
(R27)	$CH_3O_2H + h\nu \rightarrow CH_3O + OH$	1
(R28)	$CH_3O_2H + OH \rightarrow CH_3O_2 + H_2O$	1
(R29)	$CH_2O + h\nu \rightarrow CHO + H$	1
(R30)	$CH_2O + OH \rightarrow CHO + H_2O$	2
(R31)	$CHO + O_2 \rightarrow CO + HO_2$	2
(R32)	$SO_2 + OH + M \rightarrow HOSO_2 + M$	2
(R33)	$HOSO_2 + O_2 \rightarrow HO_2 + SO_3$	1
(R34)	$SO_3 + H_2O \rightarrow H_2SO_4$	2
(R35)	$CFCl_3 + O(^1D) \rightarrow$ products	1
(R36)	$CFCl_3 + h\nu \rightarrow$ products	1
(R37)	$CF_2Cl_2 + O(^1D) \rightarrow$ products	1
(R38)	$CF_2Cl_2 + h\nu \rightarrow$ products	1
(R39)	$N_2O + h\nu \rightarrow N_2 + O(^1D)$	1
(R40)	$N_2O + O(^1D) \rightarrow 2NO$	1
(R41)	$N_2O + O(^1D) \rightarrow N_2 + O_2$	1

References: 1, *DeMore et al.* [1994]; 2, *Atkinson et al.* [1992]; and 3, *Stockwell* [1995].

meridional component of the eddy flux is parameterized in terms of a horizontal diffusion coefficient K_{yy}, assuming that the motions related to baroclinic waves are quasi-horizontal:

$$\overline{v'\Psi'} \equiv -K_{yy}\left(\frac{\partial\overline{\Psi}}{\partial y}\right) \tag{9}$$

The vertical component of the eddy flux is similarly obtained using the same formula and vertical eddy diffusion coefficient K_{zz} as proposed by *Stone and Yao* [1990] for water vapor.

To eliminate numerical noise and correct an apparent underestimate of the horizontal eddy fluxes in the tropical regions, we applied a second-order horizontal diffusion term in the model with a constant diffusion coefficient K_H of 8×10^5 m^2/s, which is significantly smaller than the typical eddy coefficients of 2-4 $\times$ 10^6 m^2/s in midlatitudes. Sensitivity runs have shown that without this diffusion term, the model produces gradients of the passive tracer $CFCl_3$ defined by the differences between mole fractions in the midlatitudes of the northern and southern hemispheres, which are too high compared with observations. Runs with this added weak diffusion as discussed later provide an excellent fit to this gradient and its evolution in time.

Table 2. Aqueous Phase Chemical Reactions Included in the Model

Number	Reaction
(R42)	$H_2SO_4(g) \Leftrightarrow H_2SO_4(aq)$
(R43)	$H_2SO_4(aq) \Leftrightarrow HSO_4^- + H^+$
(R44)	$HNO_3(g) \Leftrightarrow HNO_3(aq)$
(R45)	$HNO_3(aq) \Leftrightarrow NO_3^- + H^+$
(R46)	$CH_2O(g) \Leftrightarrow CH_2O(aq)$
(R47)	$SO_2(g) \Leftrightarrow SO_2(aq)$
(R48)	$SO_2(aq) \Leftrightarrow HSO_3^- + H^+$
(R49)	$HSO_3^- \Leftrightarrow SO_3^= + H^+$
(R50)	$H_2O_2(g) \Leftrightarrow H_2O_2(aq)$
(R51)	$HO(g) \Leftrightarrow HO(aq)$
(R52)	$HO_2(g) \Leftrightarrow HO_2(aq)$
(R53)	$HO_2(aq) \Leftrightarrow H^+ + O_2^-$

All rate constants are from *Pandis and Seinfeld* [1989].

Vertical transport of chemical species by dry and moist convection is included, as well as vertical mixing by turbulence in the planetary boundary layer. These subgrid-scale processes are both treated using the same schemes used for water vapor in the climate model [*Hansen et al.*, 1983].

2.3. Chemistry and Deposition

There are 41 gas-phase and 12 heterogeneous reactions in the model. The gas-phase chemistry has three major parts: tropospheric O_3-HO_x-NO_x-CO-CH_4 reactions (following *Crutzen and Zimmermann* [1991]); tropospheric SO_2-sulfate reactions; and stratospheric chlorofluorocarbon and N_2O removal reactions (Table 1). In its present form, the chemistry model uses specified stratospheric photochemical destruction rates computed off-line in recent runs of a global three-dimensional stratospheric model [*Golombek and Prinn*, 1986, 1993]. The latter destruction rates yield global atmospheric lifetimes of 46 years for $CFCl_3$, 120 years for CF_2Cl_2, and 150 years for N_2O. The current version of the model does not include prediction of stratospheric ozone chemistry, primarily due to the limited vertical spatial resolution of the model stratosphere.

We use the Livermore solver for ordinary differential equations, or LSODE [*Hindmarsh*, 1983], with certain modifications, to solve the characteristically stiff ordinary differential equations involved in modeling the tropospheric chemistry. To reduce the size of the matrix to be inverted in LSODE, we assume a quasi steady state for the atoms and free radicals with very short lifetimes (e.g., $O(^3P)$, $O(^1D)$, H, NO_3, CH_3, CHO, CH_3O, CH_3O_2, $HOSO_2$, and SO_3). Tests of the quasi steady state assumption have been carried out using both a zero-dimensional "box" gas-phase chemistry model and our fully coupled climate and chemistry model. These tests show that the simplified version with quasi steady states provides results very similar to a more comprehensive version without these approximations and greatly reduces the computational time.

The cloud and precipitation scheme is the same as used in the parent model [*Hansen et al.*, 1983]. Dissolution of soluble gases in precipitating water is included in the wet deposition term in the model (Table 2), and the precipitating water is removed at each time step assuming no further aqueous reactions such as aqueous phase oxidations of SO_2 by H_2O_2 and O_3. The initial *p*H value of solution is 5.6, to be in equilibrium with the current atmospheric CO_2 concentration. These simplifications will most likely lead to underestimates of the scavenging of SO_2 and conversion of SO_2 to sulfate. We also assume that the only important loss mechanisms for HNO_3 and N_2O_5 are scavenging by precipitation (i.e., we neglect their photodissociations). The impact of heterogeneous reactions therefore is primarily on the gaseous phase component of chemical species. For a chemical species, the ratio of its gaseous phase to its aqueous phase component is [*Seinfeld*, 1986]:

$$r = \frac{M(aq)}{M(g)} = \frac{HpL}{p/RT} = HRTL \tag{10}$$

where M(aq) is the aqueous phase concentration and M(g) is the gaseous phase concentration, both in moles per liter of atmospheric air; p and H are the partial pressure (in atmospheres) and the effective Henry's law coefficient (mole l^{-1} atm^{-1}), respectively, of the species; R is the gas constant (0.082 atm mole l^{-1} K^{-1}); T is temperature in degrees Kelvin; and L is the volume of condensed water per unit volume of air, which is $\cong 10^{-3}$ times the molar mixing ratio of condensed water. If $M^0(g)$ represents the concentration of the species in the gas phase before the calculation of wet scavenging, the postscavenging gas-phase concentration M(g) can be derived from equation (10), combined with the requirement for conservation that $M(g) = M^0(g) - M(aq) = M^0(g) - r\,M(g)$ to yield

$$M(g) = \frac{M^0(g)}{1+r} \tag{11}$$

Dry deposition of some of the chemical species (NO, NO_2, HNO_3, N_2O_5, and O_3) has been formulated in this model based on previous work [*Hough*, 1991; *Kanakidou et al.*, 1991; *Hauglustaine et al.*, 1994].

2.4. Carbon Sinks

We have included two major net sinks of CO_2 in our model: land biospheric uptake (primarily by vegetation in the northern hemisphere) and oceanic uptake. A fixed value of 1.9 pg C/yr is assumed for the current land biospheric uptake of CO_2 consistent with *International Panel on Climate Change* (IPCC) [1994] estimates. Runs of a terrestrial ecosystem model [*Xiao et al.*, 1997] driven by rising CO_2 and changing climate have indicated that land uptake may vary with time [*Prinn et al.*, 1997]. This possibility will be addressed in later versions of the chemistry-climate model run interactively with the terrestrial ecosystem model. The oceanic uptake of CO_2 is calculated using an ocean carbon model [*Prinn et al.*, 1997], which includes inorganic chemistry in the ocean surface water and transport of dissolved inorganic carbon to the deep ocean using the same scheme as used for heat in the 2-D LO climate submodel.

The oceanic uptake of CO_2 at 22 latitudinal grid points (from 90°N to 74°S) are calculated each day by the ocean

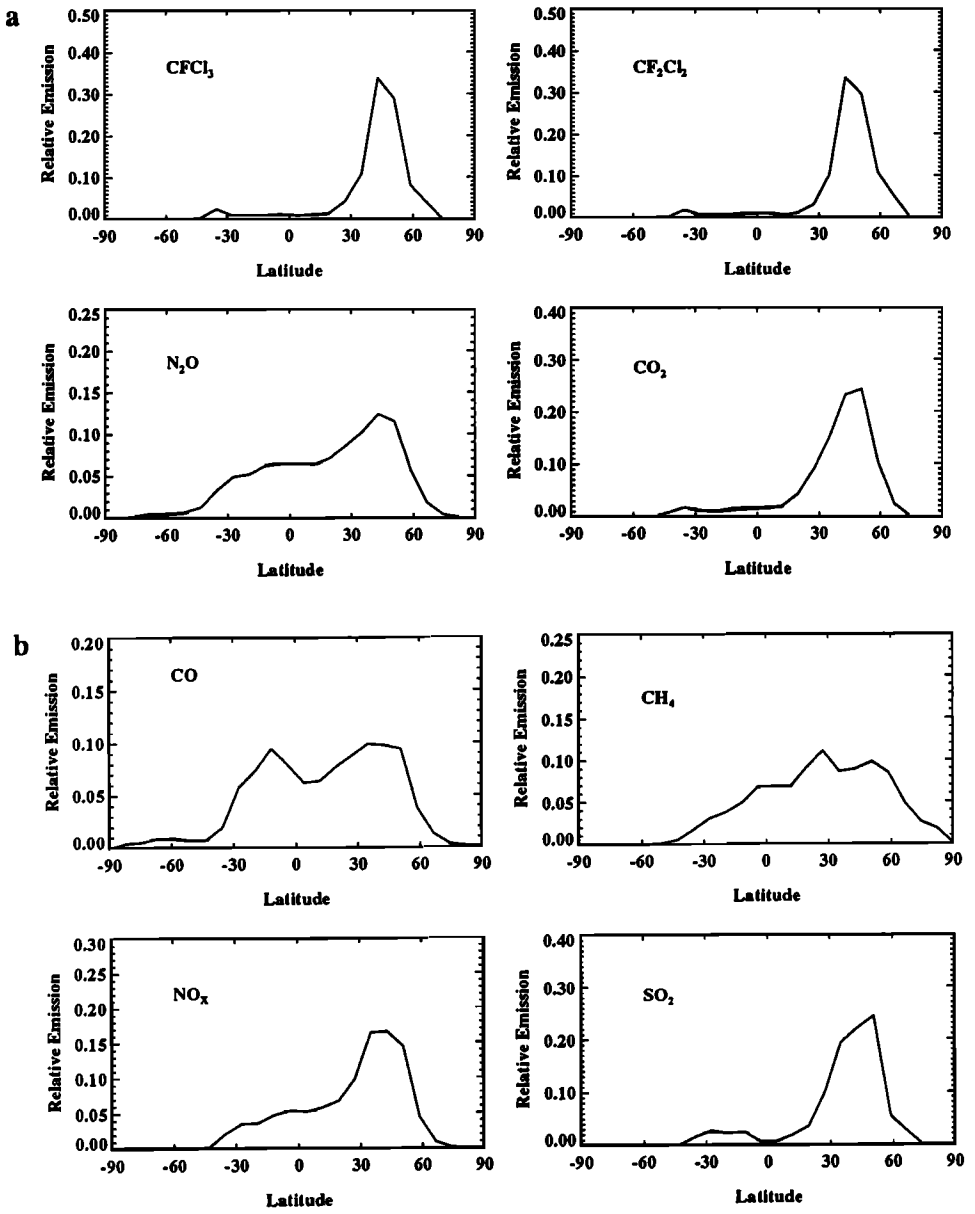

Figure 1. Latitudinal distributions of relative emissions (0-1) of (a) $CFCl_3$, CF_2Cl_2, N_2O, and CO_2 and (b) CO, CH_4, NO_x, and SO_2.

carbon submodel based on the predicted surface winds, atmospheric concentrations of CO_2, and oceanic distributions of temperature and dissolved inorganic carbons. Predicted rates of this oceanic uptake are about 2.0 pg C/yr for the 1980s and increase thereafter to 8.4 pg C/yr in 2100. In the present version of our model, the land biospheric uptake (1.9 pg C/yr) is treated by removing appropriate amounts of CO_2 hourly at each grid point of the model with no attempt to simulate the substantial seasonal cycle in this uptake.

2.5. Emissions

Emissions of CO_2, CH_4, N_2O, $CFCl_3$, CF_2Cl_2, CO, NO, and SO_2 are considered. Except for the two chlorofluorocarbons, all emissions are divided into natural and anthropogenic emissions. Both are functions of latitude and include many subcategories. Values for, and distributions of, these emissions are based on previous research: *Prinn et al.* [1990] for N_2O before 1990s; *Hartley and Prinn* [1993] for $CFCl_3$ and CF_2Cl_2 up to 1992; *Alternative Fluorocarbons Environmental Acceptability Study* (*AFEAS*) [1994] and *Fisher et al.* [1994] for $CFCl_3$ and CF_2Cl_2 after 1992; *IPCC* [1994] for CO_2; *Fung et al.* [1991] for CH_4; *Spiro et al.* [1992] for SO_2; *Hough* [1991], *Law and Pyle* [1993], and *Crutzen and Zimmermann* [1991] for CO and NO_x; and the Global Emission Inventory Activity (GEIA) data set [*Graedel*, 1994] for SO_2. Figure 1 shows the latitudinal distributions of emissions used in our simulations up to the year 1985. After 1985, latitudinal distributions of CO, NO, and SO_2 are predicted and change with time.

We treat the total annual natural emissions of CH_4, N_2O, CO, NO, and SO_2 as constants with time in the present simulations. Specifically, the assumed natural emissions of

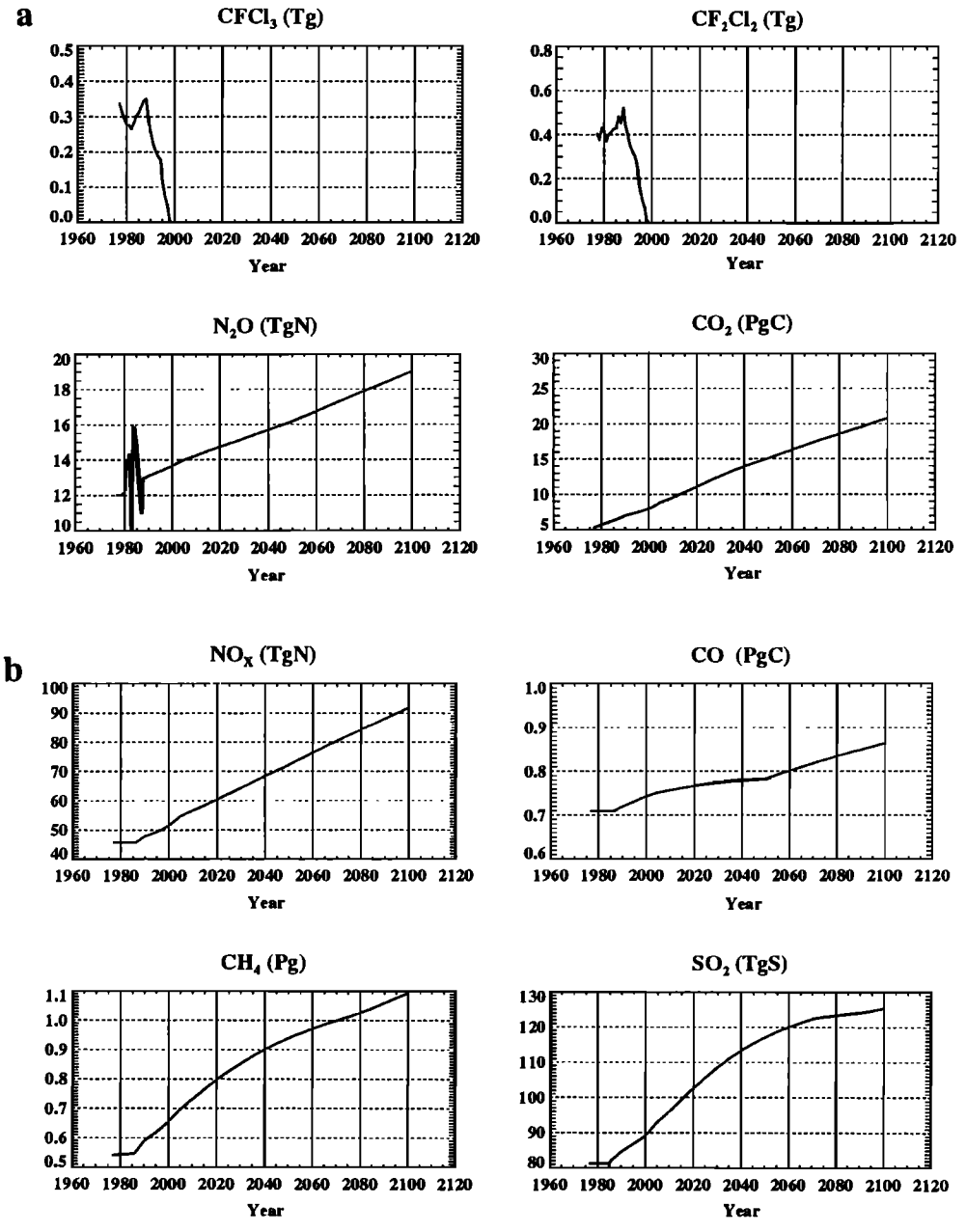

Figure 2. Annual emissions of (a) $CFCl_3$ (Tg), CF_2Cl_2 (Tg), N_2O (Tg N), and CO_2 (pg C) and (b) NO_x (Tg N), CO (pg C), CH_4 (pg), and SO_2 (Tg S).

CH_4, N_2O, CO, NO (exclusive of lightning), and sulfur are 130 Tg/yr, 9.1 Tg (N)/yr, 158.6 Tg (C)/yr, 10 Tg (N)/yr, and 12.8 Tg (S)/yr, respectively. Production of NO by lightning is assumed to be 5 Tg (N)/yr in all years but distributed as a function of both latitude and season in each year [*Kumar et al.*, 1995]. We assume that 70% of the NO produced by lightning at each latitudinal grid point is uniformly distributed into the lowest five vertical layers, and the remaining 30% is distributed into the two highest layers in the troposphere. Runs of a natural emissions model driven by changing climate and land ecosystems indicate significant changes in natural N_2O and CH_4 emissions are possible [*Liu*, 1996; *Prinn et al.*, 1997]. This will be studied in later versions of the chemistry-climate model.

The treatment of anthropogenic emissions other than chlorofluorocarbons consists of two parts: (1) from 1977 to 1985 and (2) after 1985. In the first period, our estimates are based on previous research results as listed above. For the second period the time-varying annual amounts of anthropogenic emissions predicted by the MIT emissions prediction and policy analysis (EPPA) model in 12 economic regions [*Yang et al.*, 1996] are mapped into emissions for each latitudinal grid point. For the chlorofluorocarbons, we assumed values from *Hartley and Prinn* [1993], *AFEAS* [1994], and *Fisher et al.*, [1994] for the emissions before 1994. After 1994, emissions decrease linearly to zero values after the year 2000. To achieve reasonable mixing efficiency and numerical stability, all the emissions except for those of

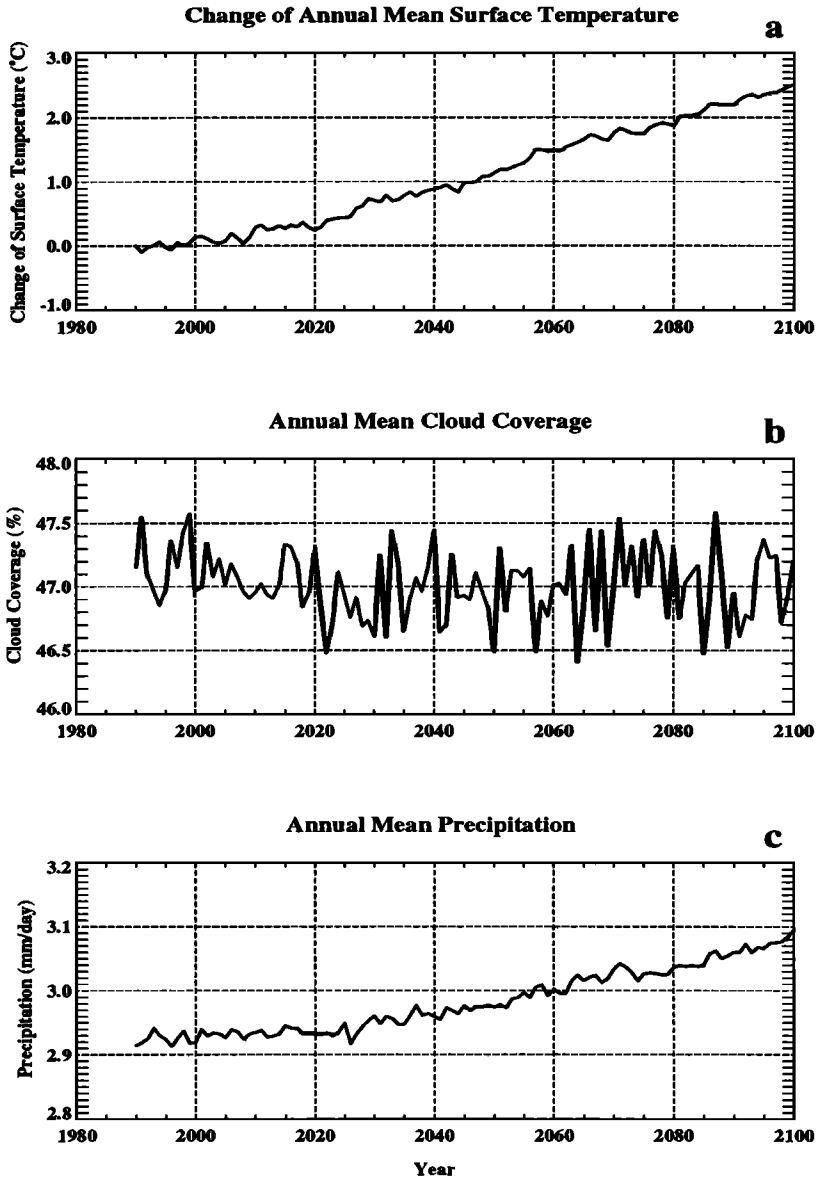

Figure 3. Model-predicted annual-mean and global-average values of (a) surface temperature (expressed as the changes from its 1990 level in °C), (b) cloud coverage (in percentage), and (c) precipitation rate (in mm/d).

NO from lightning are added uniformly each day into the lowest two layers of the model.

2.6. Coupling of Submodels

The coupling of the chemistry and climate submodels in our system is two-way (i.e., fully interactive or on-line). The advection of chemical species is driven by the predicted winds provided by the climate submodel every 20 min. The other transport processes (convection and eddy diffusion) and the wet and dry deposition rates are calculated every hour (i.e., 3 times the climate submodel time step). The gas-phase chemistry is solved with 3-hour time steps using solar radiation fluxes, temperatures, and water vapor mixing ratios calculated by the climate submodel. Predicted mole fractions of radiatively active gases, specifically CO_2, N_2O, CH_4, $CFCl_3$, CF_2Cl_2, and optical depths of sulfate aerosol, are used, in turn, every 5 hours by the climate submodel to derive their contributions to radiative forcing. In the current version of the chemistry submodel, the radiative forcing due to the predicted sulfate derived from anthropogenic SO_2 is applied as an additional forcing (both direct and indirect) to a constant background aerosol forcing in the climate submodel. It is interpreted as the additional radiative forcing due to anthropogenic sulfur emissions and is applied only to the land fraction of the climate submodel at each relevant latitude. The aerosol direct effect is computed from the predicted concentrations of sulfate aerosols. The highly uncertain indirect aerosol effect is parameterized by assuming radiative forcing by this effect is twice that computed for the direct effect without explicit inclusion of aerosol-cloud interactions, consistent with the recent *IPCC* [1996] assessment. The radiation code in the current version of the model uses prescribed ozone based on 1958-1970 observations as in the parent GISS GCM [*Hansen et al.*, 1983]. Future versions will

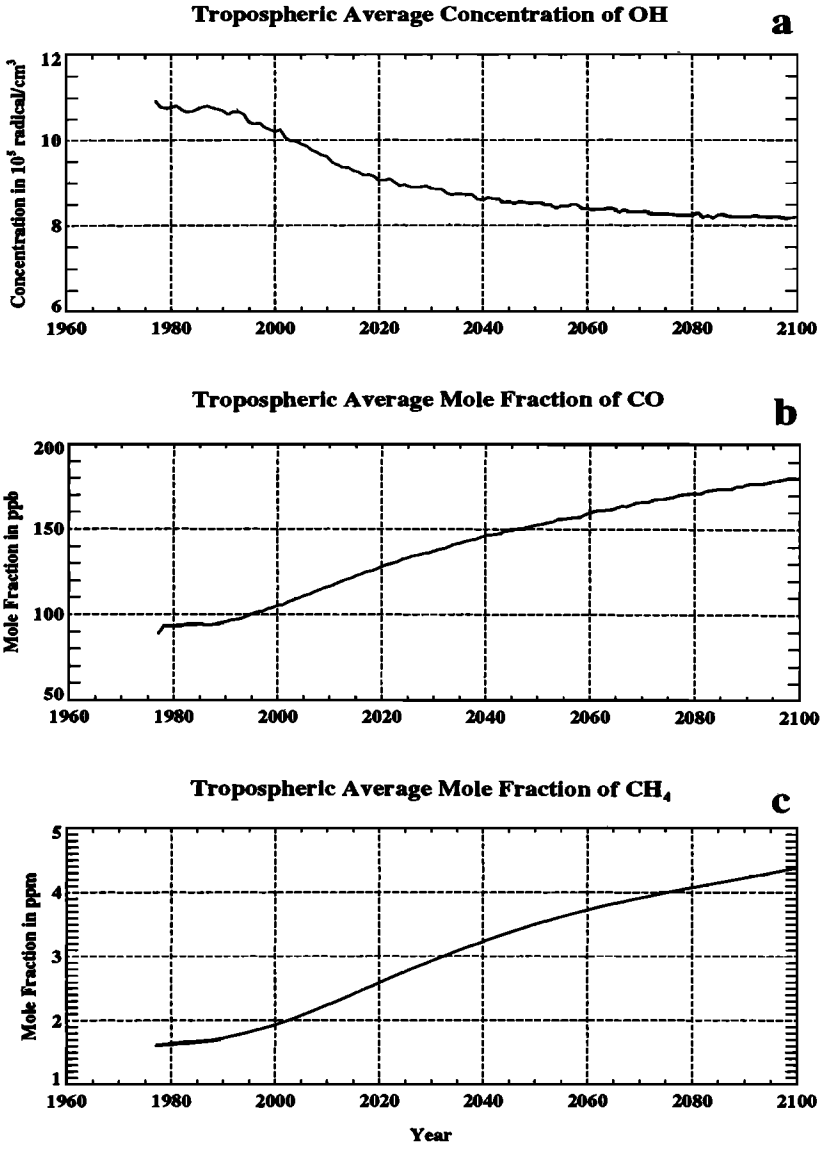

Figure 4. Model-predicted tropospheric concentrations of (a) OH (in 10^5 radicals/cm^3), (b) mole fractions of CO (in parts per billion), and (c) mole fractions of CH_4 (in ppm), as functions of time.

use tropospheric and stratospheric ozone as predicted by the model in the radiation code. Note that the radiative forcings by increasing tropospheric and decreasing stratospheric ozone partially offset one another

3. Reference Run

In order to test our model, we have carried out a transient simulation of "present-day" conditions and also a series of sensitivity tests using specified surface emissions of the relevant chemicals. The present-day simulation period begins in 1977, enabling use of observations [e.g., *Cunnold et al.*, 1994; *Novelli et al*, 1992] to compare with model results. Total integration times of these runs are 124 years (from 1977 to 2100).

Specified emissions for all the relevant species, including both natural and anthropogenic sources, used in these runs as functions of time are summarized in Figure 2. Except for those of chlorofluorocarbons, which are assumed to decline linearly after 1994, all emissions increase with time (e.g., N_2O from 12 Tg N/yr in 1977 to 19 Tg N/yr in 2100; CO_2 from 5.4 pg C/yr in 1977 to 21 pg C/yr in 2100; and CH_4 from 540 Tg/yr in 1977 to 1.1 pg/yr in 2100).

3.1. Temporal Trends

As a result of the assumed increasing emissions of long-lived gases, global average mole fractions of CO_2, N_2O, and CH_4 rise to 745 ppm, 410 ppb, and 4.4 ppm, respectively, by the year 2100. The model also predicts that if the actual reduction of $CFCl_3$ and CF_2Cl_2 emissions is the same as we assume in the model, the global average $CFCl_3$ and CF_2Cl_2 mole fractions will decrease to their 1977 levels around 2030 and after 2090, respectively (the difference between the two being due to the much longer lifetime of CF_2Cl_2).

Climate submodel results (Figure 3) show that the global average surface temperature increases by about 2.5°C between 1990 and 2100. This increase is due to the increased radiative forcing of the trace gases and subsequent climate-model

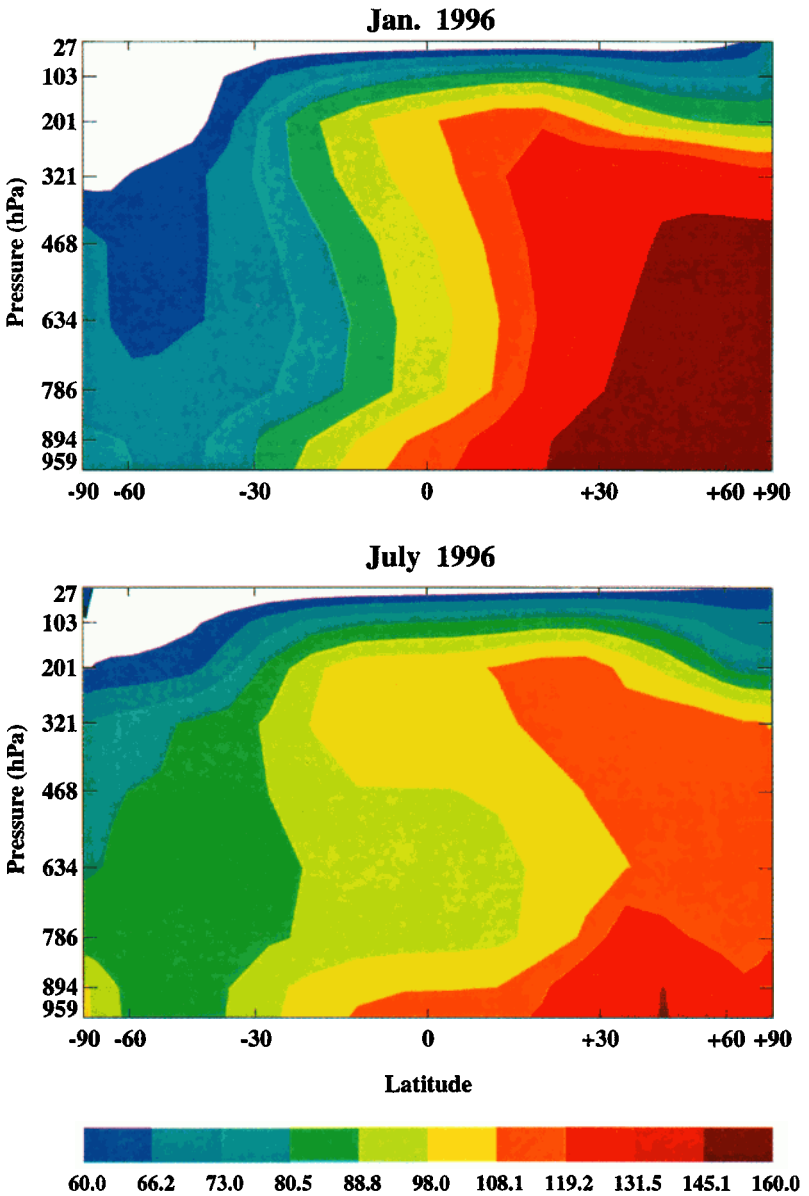

Plate 1. Model-predicted latitudinal and vertical distributions of zonal average mole fractions of CO (parts per billion) in (top) January and (bottom) July of 1996.

feedbacks and occurs despite the slightly enhanced cooling effect of increasing sulfate aerosols over this time. Global-mean annual cloud coverage is predicted to drop by about 0.5% by the end of next century, while the global-mean annual precipitation increases from 2.92 mm/d in 1990 to 3.10 mm/d in 2100. Details of other aspects of climate change patterns and impacts predicted by the 2-D LO model are given by *Prinn et al.* [1997].

Increases similar to the ones for the long-lived species are found for several short-lived species including CO, NO_x, SO_2, and sulfate, again driven primarily by their increased emissions. For example, the tropospheric average mole fraction of CO is predicted to be 180 ppb in 2100, which is about double the current value. For NO_x, in the lower atmosphere, wintertime surface mole fractions in midlatitudes of the northern hemisphere rise from 420 ppt in 1996 to 885 ppt in 2100. Increased emissions of SO_2 (57% according to Figure 2b) are offset somewhat by increased wet deposition associated with predicted rainfall increases. The maximum monthly mean value of the SO_2 surface mole fraction as seen in the midlatitudes of the northern hemisphere increased by about 18% from 1996 to 2100, while the same parameter for sulfate increased by about 42% during the wintertime and almost doubled in the summertime. Opposite to the trends of most short-lived species, the concentration of tropospheric OH, the most important oxidizing species in the lower atmosphere, is predicted to decrease by about 20% between 1990 and 2100 (Figure 4). The decrease is due to the predicted increases of CH_4 and CO emissions (Figure 2b) and hence concentrations (Figure 4), offset by increased NO_x emissions and modulated by changes in temperature and humidity.

3.2. Spatial Distributions

As expected, many short-lived species are predicted to have very strong spatial and seasonal variability. Predicted present-

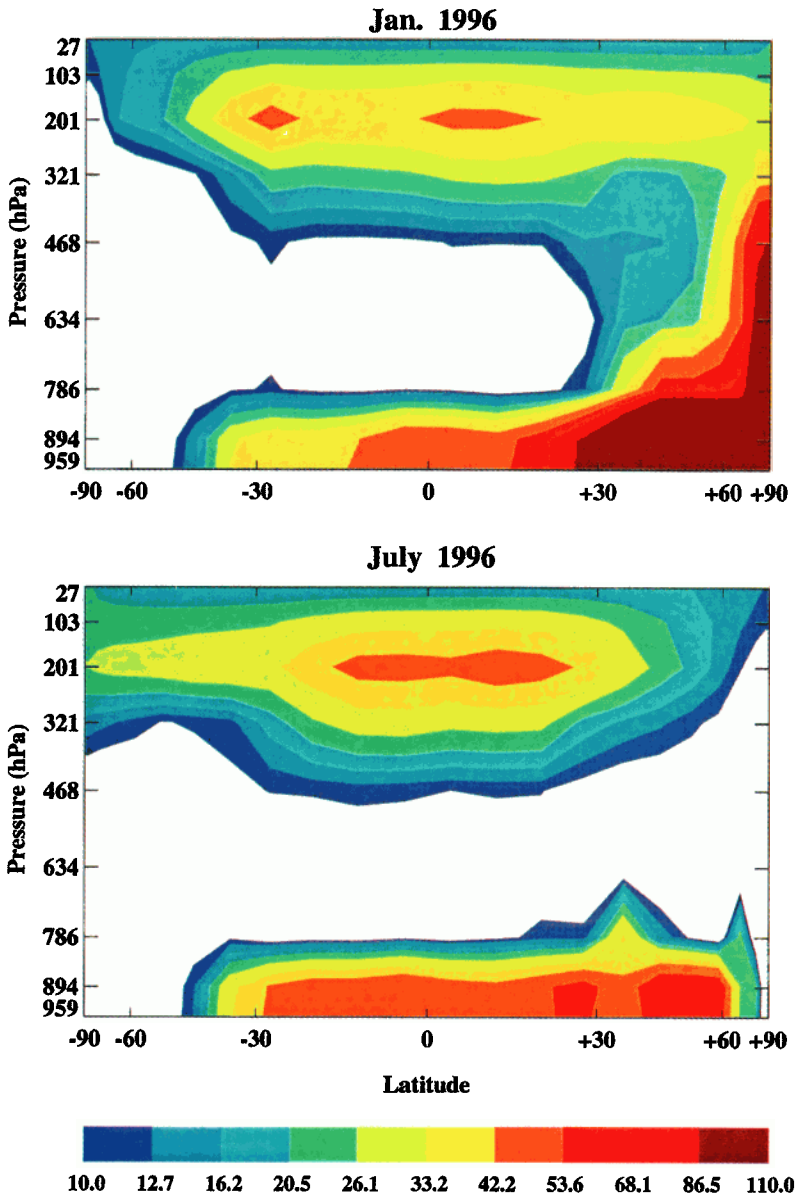

Plate 2. The same as in Plate 1, except for NO_x (parts per trillion).

day CO concentrations for the northern hemisphere are much higher during the wintertime than the summertime (Plate 1). Specifically, the peak value of the CO mole fraction in the middle and upper troposphere in the northern hemisphere is about 40 ppb lower in the summer than the winter. This seasonal difference, caused by more rapid summertime removal of CO, also affects the tropical region. Specifically, tropical and northern subtropical CO concentrations are much higher in northern hemisphere winter than summer at all tropospheric levels. Note also that due to predicted high concentrations of OH in the tropics, CO concentrations in the tropical region are lower than those even in the free troposphere over the northern hemisphere despite significant tropical CO emissions (Figure 1b).

The modeled NO_x ($NO + NO_2$) pattern has a similar seasonal variability to CO in the lower atmosphere in the northern hemisphere (Plate 2). In addition, a very interesting feature of the predicted NO_x distribution is the appearance of a band of relatively high NO_x around the tropopause at low latitudes, which changes little between seasons. The source of this band is both transport of NO_x from the lower atmosphere and local production by lightning. Similar distributions with even higher mole fractions of NO_x in the upper troposphere are found in several regional observations [e.g., *Ehhalt et al.*, 1992; *Singh et al.*, 1996]. Note that the model does not include stratospheric downward transport of either NO_x or NO_y, and this may be what causes the difference between the observations and our model's results. Lacking observational data for tropical upper tropospheric NOx with reasonably large coverage, we cannot confirm the reality of this prediction at this moment, although it turns out to be consistent with recent three-dimensional model results [*Levy et al.*, 1997; *Jaffe et al.*, 1997].

Regions with predicted high mole fractions of OH switch

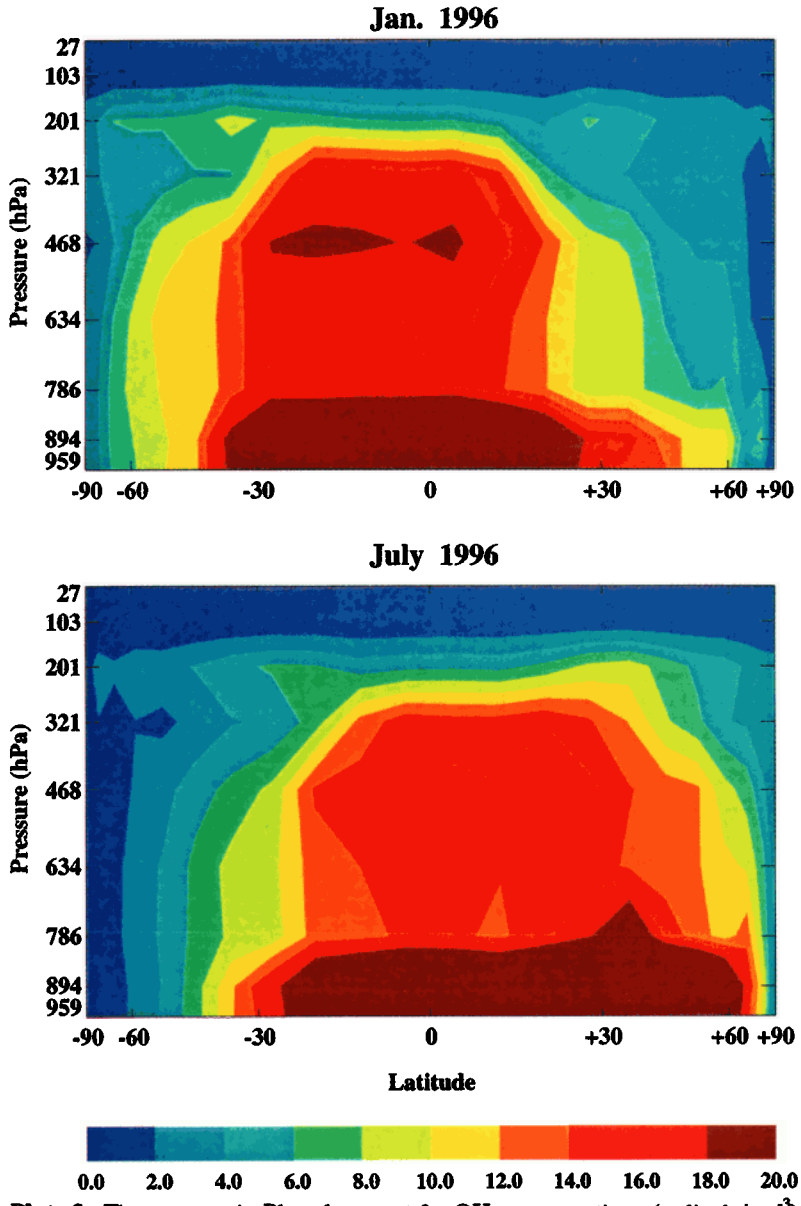

Plate 3. The same as in Plate 1, except for OH concentrations (radicals/cm^{-3}).

from the northern hemisphere summer to the southern hemisphere summer, following the movement of the tropical convective zone (Plate 3). The high OH in the tropical upper troposphere results from the enhanced NO_x levels and ultraviolet fluxes as well as ample H_2O and O_3 levels. Note that the concentrations predicted for OH in the upper troposphere are somewhat lower than those estimated by *Prinn et al.* [1995], which are based on CH_3CCl_3 observations.

From Plate 4 we see that the seasonal variations of the SO_2 distribution are not as dramatic as those for CO and NO_x, particularly in lower troposphere (below 634 hPa). Because the major sinks of SO_2 in this model are the conversion to sulfate and wet deposition, we can therefore draw the conclusion that the combination of these two processes approximately balances both regionally and seasonally the emissions of SO_2 (see Figure 1b). In contrast to this pattern, the sulfate distribution is quite different in different seasons (Plate 5). The primary reason is the seasonal variation in its production by the OH, SO_2 reaction and its very high solubility. Strong wet scavenging of sulfate gives it a short lifetime in the atmosphere, and the long-range transport of sulfate is therefore negligible. We find that simulated distributions of SO_2 and sulfate are in general agreement with observations summarized by *Chin et al.* [1996], i.e., mole fractions of SO_2 and sulfate are higher than 1 ppb in industrial regions and range from 10^1 to 10^2 ppt in remote areas.

4. Comparison with Observations

4.1. Long-Lived Species

Long-lived species, such as $CFCl_3$, CF_2Cl_2, N_2O, and CO_2, are predicted and observed to be generally well mixed vertically in the free troposphere. Latitudinal gradients of their concentrations exist, however, because of the latitudinal distributions of their sources with the magnitude of the gradient dependent upon the rate of north-south transport. Therefore comparisons of their observed and predicted surface mixing ratios as functions of latitude and time are a very good measure of the accuracy of horizontal transport rates in the model, provided the latitudinal distributions of emissions are

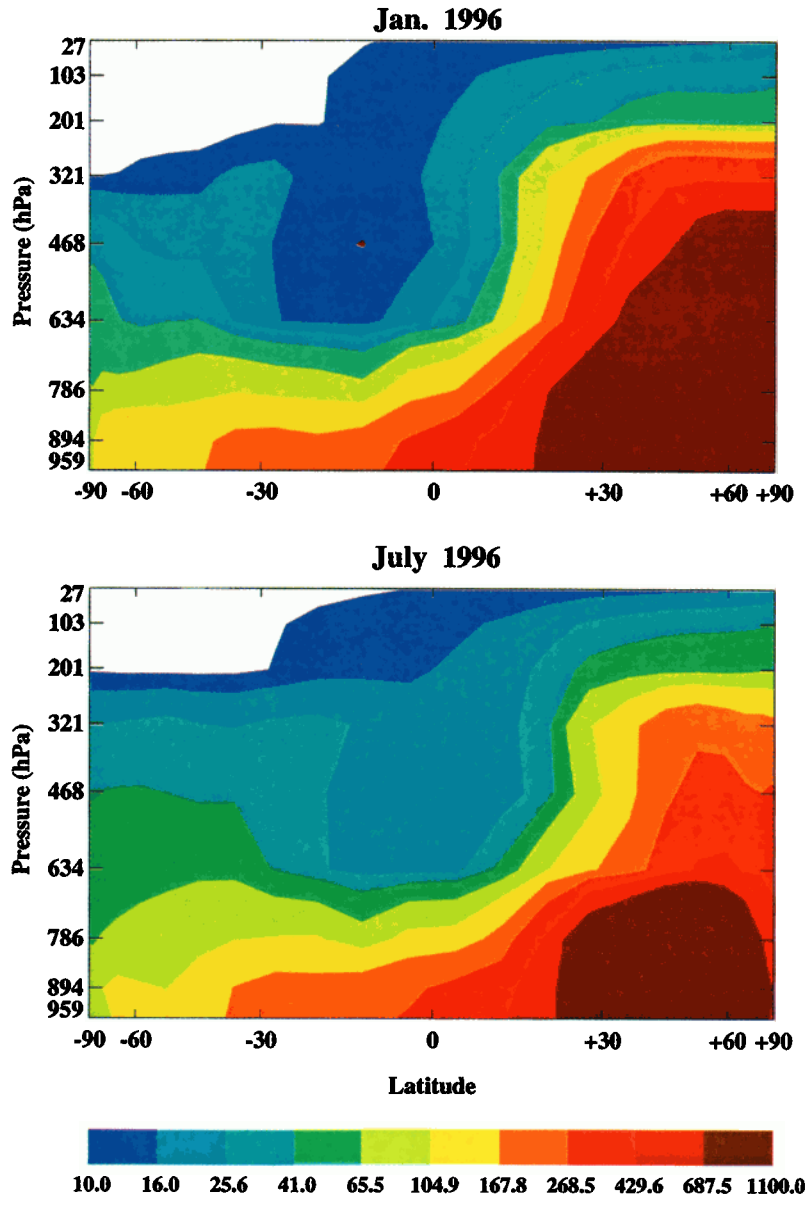

Plate 4. The same as in Plate 1, except for SO_2 (parts per trillion).

known. For this purpose, we have used the emissions discussed in section 2.5 together with monthly-mean measurements from the surface networks of the Atmospheric Lifetime Experiment (ALE)/Global Atmospheric Gases Experiment (GAGE)/Advanced Global Atmospheric Gases Experiment (AGAGE) (for $CFCl_3$, CF_2Cl_2, and N_2O) and the National Oceanic and Atmospheric Administration's Climate Monitoring and Diagnostics Laboratory (NOAA/CMDL) (for CO_2) to compare with the outputs of our model at the same latitudes and times.

We found that simulated temporal trends and latitudinal gradients in $CFCl_3$ and CF_2Cl_2 surface mole fractions agree very well with observations at the five ALE/GAGE/AGAGE stations (Figures 5 and 6). Because the sources of these two chlorofluorocarbons are predominately in the northern hemisphere, this agreement demonstrates that the simulation of interhemispheric transport in the model is quite reasonable. The variations in time of the predicted and measured latitudinal gradients of these species (as measured by the difference between the Ireland and Tasmania stations) also agree very well; for $CFCl_3$ this difference has decreased both in the model and in observations from 15-20 ppt before 1990 to 5 ppt in 1995, consistent with the rapid reduction in northern hemisphere emissions of this compound. The good agreement between predicted and observed global average concentrations indicates that the model parameterization for stratospheric losses of these species is also reasonable.

The vertical distributions of long-lived species predicted in the model have been compared with three balloon observations at 44°N (June 20, 1989 and November 5 and 10, 1990) by U. Schmidt and coworkers as reported by *Fraser et al.* [1994]. The model data were averaged values from June 1989 to November 1990. For the comparison, both observational and modeled mole fractions were expressed

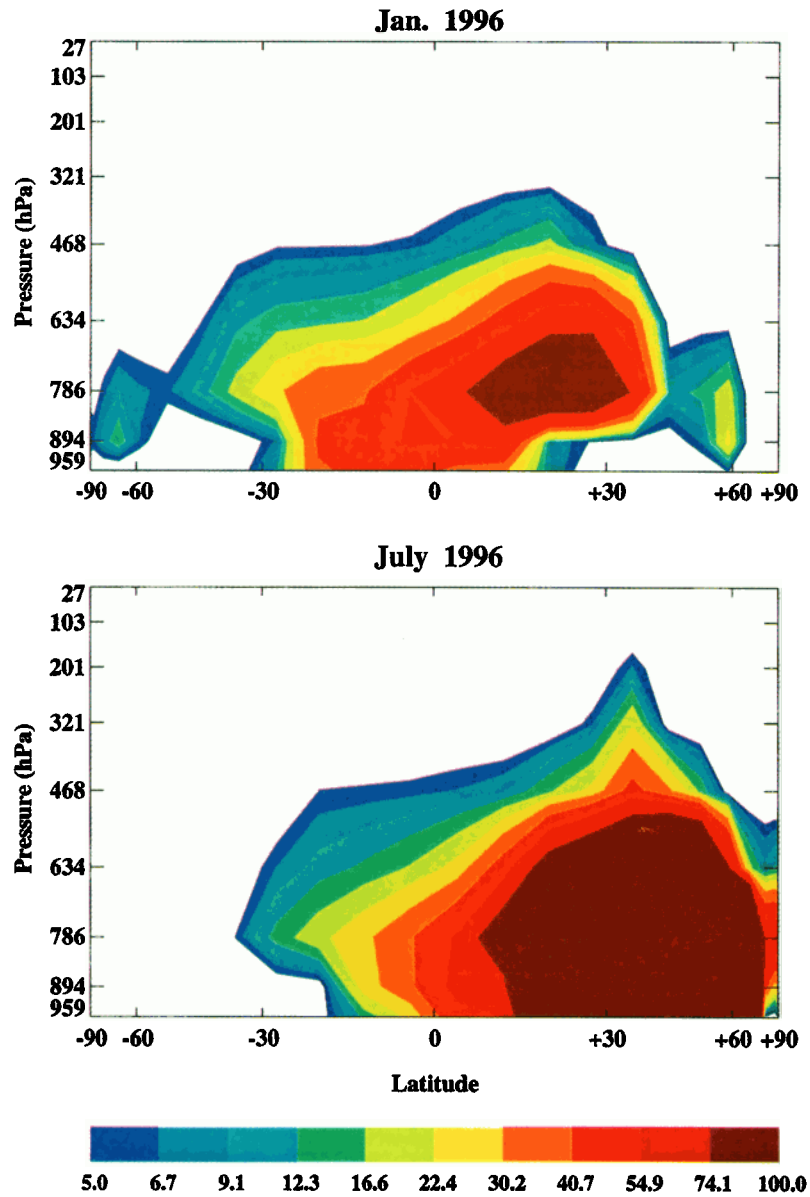

Plate 5. The same as in Plate 1, except for H_2SO_4 (parts per trillion).

relative to the maximum values in each profile (Figure 7). The observed and modeled $CFCl_3$ profiles so normalized are quite close in shape, although differences as high as 10% can be found at some levels.

Our model also predicts trends of the surface mole fractions of N_2O which are close to the ALE/GAGE/AGAGE observations, especially in the southern hemisphere and the tropics (Figure 8). In the northern hemisphere midlatitudes, the simulated N_2O mixing ratios are generally lower than the observed ones, although the predicted trends are still similar to observations. A probable reason for this result is underestimation of the N_2O emissions in the northern hemisphere midlatitudes.

The model predicts oceanic uptake of carbon dioxide (~2.0 pg C/yr for the 1980s) close to the values predicted in the more detailed models (e.g., 1.81 pg C/yr of *Sarmiento et al.* [1992] and 2.1 pg C/yr of *Orr* [1993]; both are for the 1980s), and together with the assumed terrestrial CO_2 uptake, this leads to predicted trends for the surface mole fractions of CO_2 close to those observed at five globally distributed NOAA/CMDL stations (Figure 9). Note that the seasonal cycles in predicted concentrations are due to transport and oceanic uptake only. The seasonal cycle in the net terrestrial biospheric flux (positive in fall and winter and negative in spring and summer in the northern hemisphere) is not included as noted earlier. Fully interactive coupling of the ecosystem model with the current chemistry-climate model is under way and hopefully will provide a realistic representation of this missing cyclical process.

4.2. CH_4 and CO

When compared with the ALE/GAGE/AGAGE network measurements, the surface mole fractions of CH_4 predicted in our model are generally quite close to the observations but are somewhat higher (by up to 0.1 ppm) than measured results at

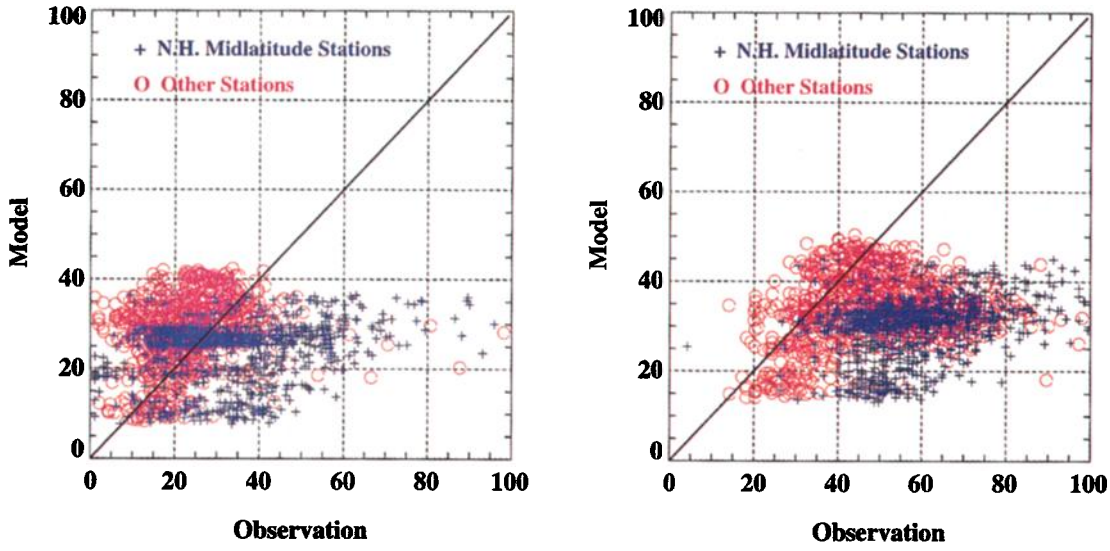

Plate 6. Comparisons between modeled and observed ozone mole fractions (parts per billion) at (left) surface and (right) 500-hPa levels. Data from the northern hemisphere midlatitudes are marked by red circles, and data from other stations are marked by blue plus signs. Observational data are from 22 ozone sounding stations archived in the World Ozone Data Center.

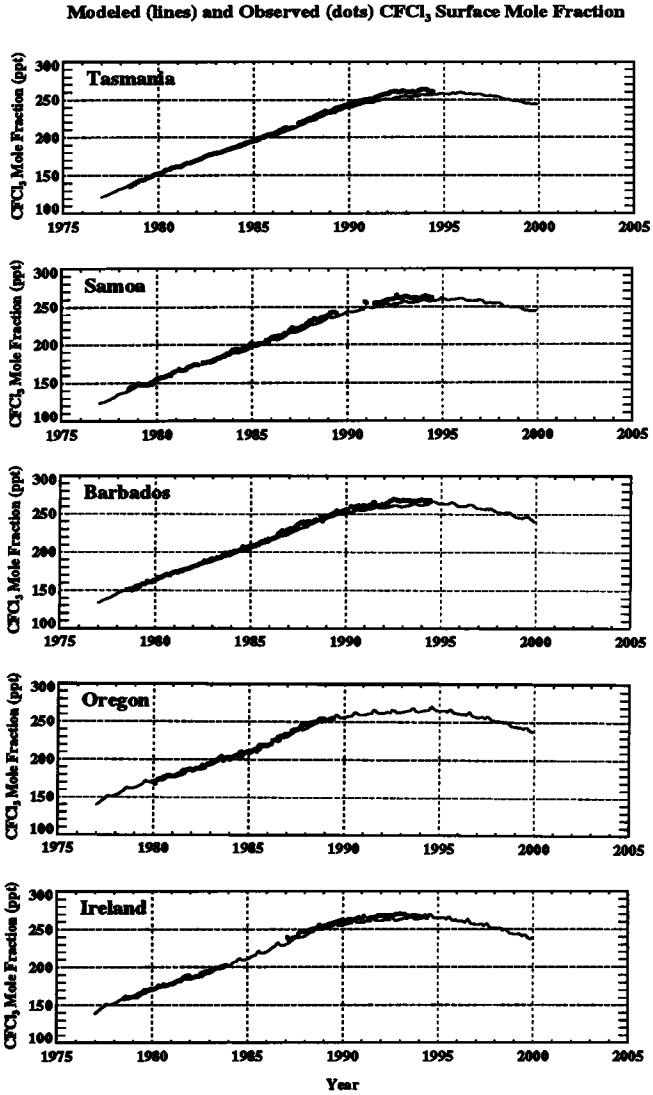

Samoa, Barbados, Oregon, and Ireland (Figure 10). Overprediction of CH_4 could be related to overprediction of annual-average emissions or underprediction of annual-average OH levels in the northern hemisphere. Predicted seasonal cycles at all five stations agree fairly well with observations, indicating that the predicted seasonal cycles in transport and OH concentrations at the latitudes of these stations are quite realistic.

The major sink for atmospheric carbon monoxide is also reaction with OH, and its lifetime is much shorter (months) relative to methane (8.3 years, [*Prinn et al.*, 1995]). Therefore zonal variations (of course, not included in our model) are much larger for CO than for the long-lived species. The most we can expect from our zonal-mean model is an adequate simulation of latitudinal gradients and seasonal cycles in CO. Hence model predictions and observations for CO at stations at specific longitudes are not expected to agree closely. We find, in fact, that the predicted annual-average mole fractions and seasonal variations of CO are more reasonable in the northern hemisphere than the southern hemisphere (Figure 11; observational data are from the NOAA/CMDL network [see *Novelli et al.*, 1992]). Specifically, the model simulates the phase of the seasonal cycles at Alaska, Colorado, Mauna Loa, and Tasmania but underpredicts the amplitude of these cycles at Mauna Loa. Overprediction of annual average concentrations, particularly in the tropics and southern hemisphere could be due to underprediction of OH or to the assumed CO sources in these regions in the model being too

Figure 5. Comparisons between model-simulated (lines) and observed (dots) surface mole fractions of $CFCl_3$ (parts per trillion) at five Atmospheric Lifetime Experiment (ALE)/Global Atmospheric Gases Experiment (GAGE)/Advanced Global Atmospheric Gases Experiment (AGAGE) stations.

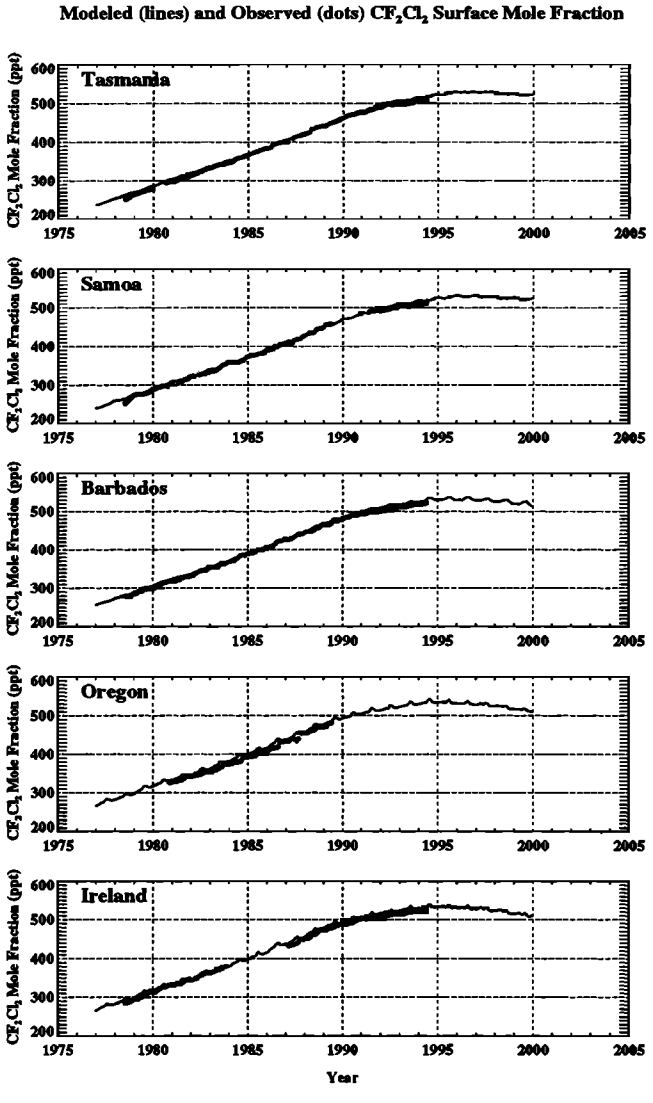

Figure 6. The same as in Figure 5, except for CF_2Cl_2 (parts per trillion).

large. It is interesting to note that a similar overestimation in simulating short-lived species is also found in other zonally averaged models [e.g., *Derwent*, 1996].

4.3. Tropospheric Ozone and OH

Ozone is one of the key species in tropospheric chemistry. However, owing to its sometimes rapid in situ production and short lifetime in the troposphere, an adequate measurement network for tropospheric ozone requires fairly high spatial and temporal resolution and a carefully designed distribution of stations [*Prinn*, 1988]. Currently, such a network does not exist globally, but there are some observations available which are useful for partial model testing.

We specifically use the ozone sounding data archived in the World Ozone Data Center for 22 selected stations which were operated after the late 1970s and covered a wide range of latitudes to compare with our model. Since the launching times and data retrieval levels are not standardized in the data set, we choose the surface and the 500-hPa levels for comparisons because both appeared in most launch records. We then derive the monthly means of these observations in order to compare with our modeling results at the same time and location (both latitudinally and vertically).

Plate 6 shows the correlation between model and observations. In the surface layer, data are generally symmetrically distributed about the linear relation line, but data from midlatitude northern hemisphere stations (marked by blue plus signs) are less so distributed than for other stations (marked by red circles). It indicates that although the model not surprisingly overestimates or underestimates ozone concentrations at some specific stations and times, it does reproduce the general climatology of the latitudinal distribution of ozone outside of polluted regions. At the 500-hPa level, the model clearly underestimates O_3 mole fractions in the northern hemisphere midlatitudes but is again closer to observations in other regions. One plausible reason for these results is the geographical location of the stations. Since most of these stations are located in urban areas or close to urban areas, they may be poor representations of the zonal averages predicted in our model at polluted latitudes.

Model-simulated ozone mole fractions reach their peak values during summer at both the surface and 500 hPa in the southern hemisphere. In the northern hemisphere, simulated ozone mole fractions have two peaks at the surface (appearing

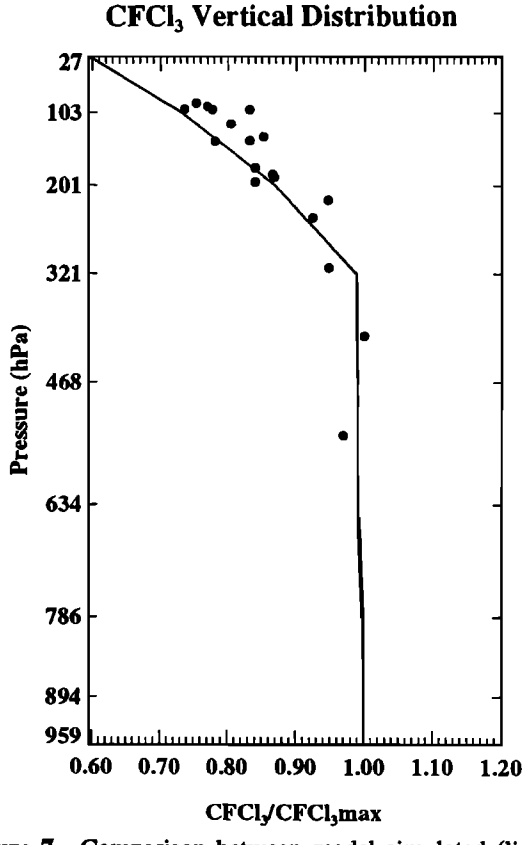

Figure 7. Comparison between model simulated (line) and observed (dots) vertical profiles of $CFCl_3$ at 44°N. Observational data are from three balloon observations (June 20, 1989 and November 5 and 10, 1990) by U. Schmidt and coworkers as reported by *Fraser et al.* [1994]. The model data are averaged values from June 1989 to November 1990. Both observational and modeled concentrations are expressed relative to the maximum values in each profile ($CFCl_3$/maximum $CFCl_3$).

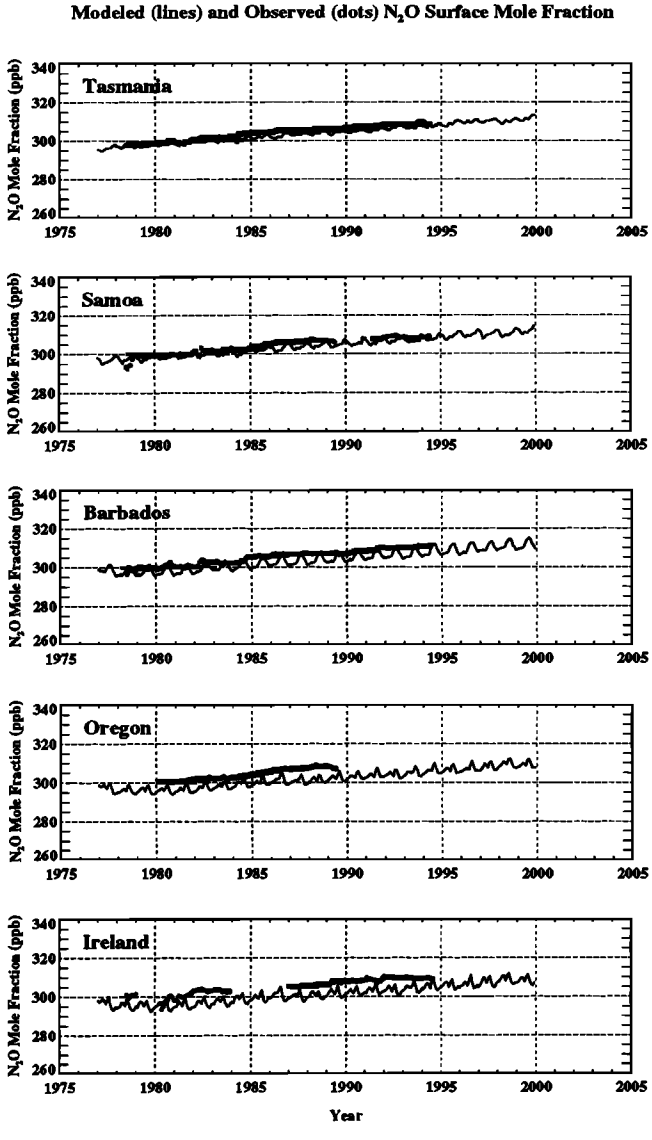

Figure 8. The same as in Figure 5, except for N_2O (parts per billion).

in late spring and midsummer, respectively) and only one peak at 500 hPa (appearing in winter). These features are in general agreement with observations [*Logan*, 1994].

As a chemical cleaner and reaction mediator, OH is arguably the most important free radical in atmospheric chemistry. The globally averaged OH concentration in the troposphere in our model for the current time (1995) is 10.4×10^5 radicals/cm^3, which is quite close to the most recent estimate of $(9.7 \pm 0.6) \times 10^5$ radicals/cm^{-3} based on measurements of CH_3CCl_3 [*Prinn et al.*, 1995]. More detailed analysis indicates that the model slightly overestimates OH concentrations in the lower troposphere but underestimates them in the upper troposphere compared with the concentrations deduced in the eight tropospheric boxes of the *Prinn et al.* [1995] analysis. Overall, the OH distributions predicted by this model provide reasonable simulations of OH-sensitive species as shown for CH_4 and CO in the earlier section and also in an independent study using our model for CH_3CCl_3 (J. Huang, personal communication, 1997).

5. Conclusions

In order to investigate interactions between long-term changes in anthropogenic emissions and climate and biogeochemical processes, we have developed a zonally averaged two-dimensional model including coupled biogeochemical and climate submodels. This model is itself a part of the MIT integrated global system model (IGSM) [*Prinn, et al.*, 1997]. This model takes emissions of multiple gases from both anthropogenic and natural sources as inputs and predicts transport, photochemical rates, and deposition fluxes in order to simulate evolution of many radiatively and chemically important species in the atmosphere. Predicted concentrations of chemical species are used in an interactive procedure to calculate radiative forcing in the climate submodel. In the study of the centennial-scale climate change problem, the model has been shown to be a numerically efficient tool while retaining most of the important processes in a self-consistent and comprehensive way.

As shown from the results of a "reference" run designed to be comparable to the IPCC 1992a emission scenario (IS92a)

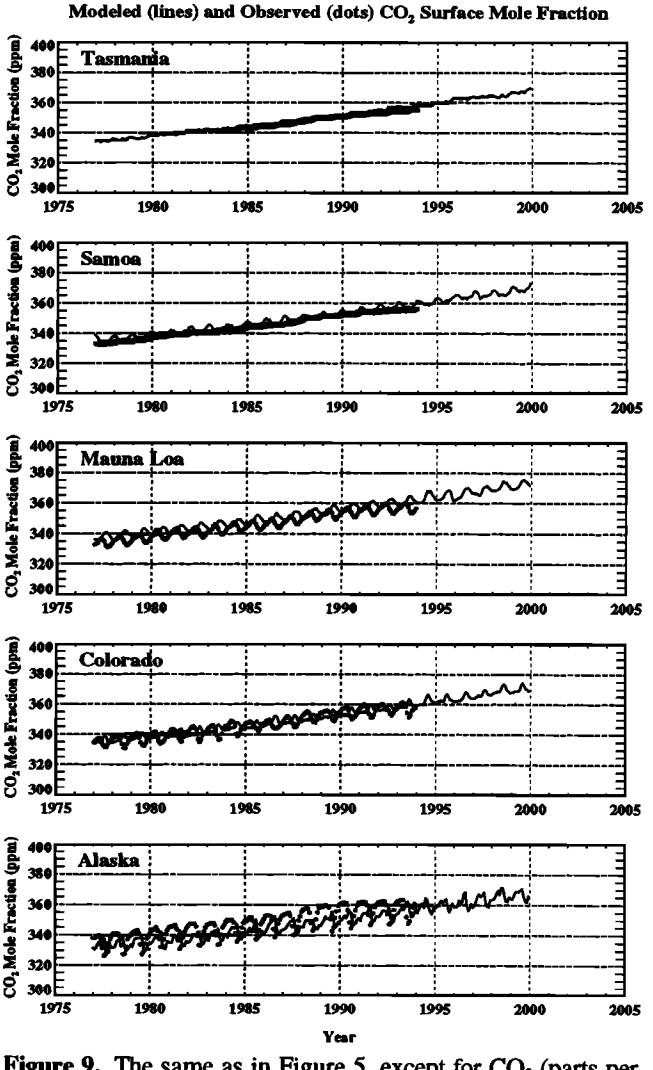

Figure 9. The same as in Figure 5, except for CO_2 (parts per million) at five National Oceanic and Atmospheric Administration's Climate Monitoring and Diagnostics Laboratory (NOAA/CMDL) stations.

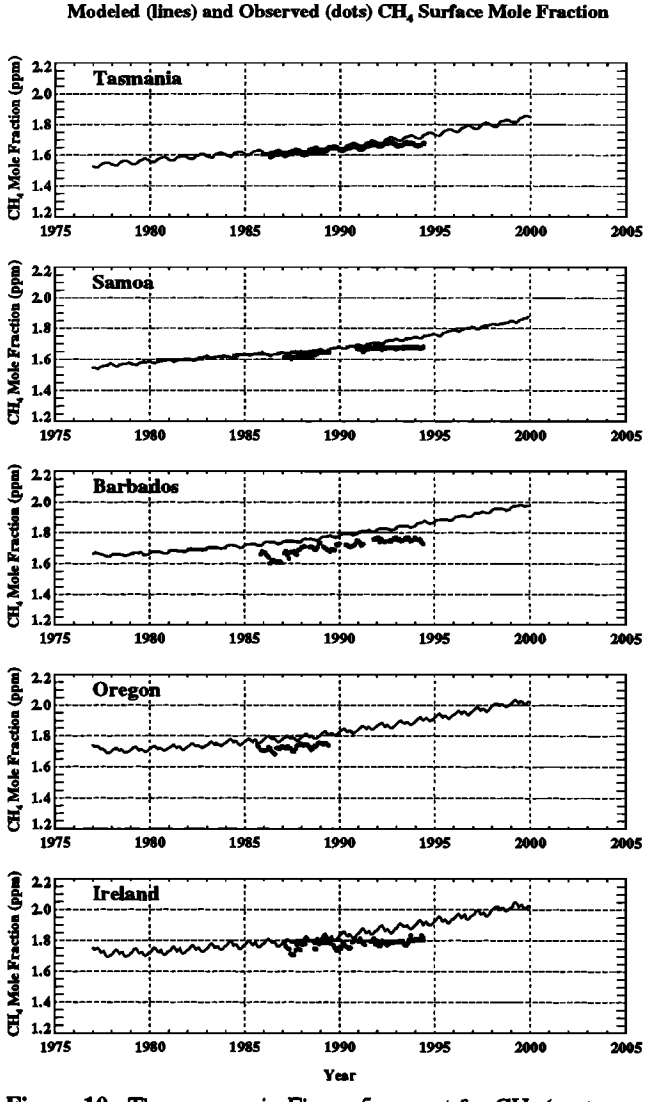

Figure 10. The same as in Figure 5, except for CH_4 (parts per million).

for CO_2 emissions, significant changes in concentrations of climate-relevant gases and hence in climate variables are predicted. The modeled current-day multiyear surface trends of several key long-lived species are generally close to observational data. Simulated vertical distributions of long-lived species are also in reasonable agreement with observations. For shorter-lived species, a direct comparison between modeled results and individual station measurements shows differences that we believe can be attributed in part to the zonal averaging in the model and in part to emission uncertainties. At the same time, this model provides reasonable simulations of seasonal variability and good agreement with observations in high northern latitudes. The agreements, where they exist, do not of course guarantee that the model will exactly represent the future evolution of the atmosphere. It does, however, provide some confidence in the transport and chemistry along with other features in the model and also provides a platform for analyzing sensitivities and uncertainties. In addition, this model should be a useful tool for analyzing policies proposed to lower emissions.

Modeled results indicate that if the current increasing trends of anthropogenic emissions of climate-relevant gases continue into the next century, the chemical structure of the atmosphere would be quite different at the end of next century than it is now. The differences include significantly higher mole fractions in 2100 of major trace gases such as CO_2 (745 ppm), N_2O (410 ppb), and CH_4 (4.4 ppm), lowered concentrations of tropospheric OH radicals (20% decrease from the current level), and almost doubled mole fractions from the current levels for the shorter-lived species CO and NO_x. As a result of this modified chemical composition, we predict a significantly warmer climate and increased precipitation, despite the cooling effect of aerosols included in the model.

Among the more interesting results from this model is the quantification of the two-way feedback between climate dynamics and atmospheric chemistry. Changes in climate, specifically in H_2O, temperature, and rainfall, provide different photochemical production and loss rates for many chemical species, while modified chemical concentrations in the atmosphere also significantly impact the climate. We will discuss these results in more detail in another paper.

It is obvious that there are many uncertainties in a model of this type. These uncertainties include, to name a few, effects of

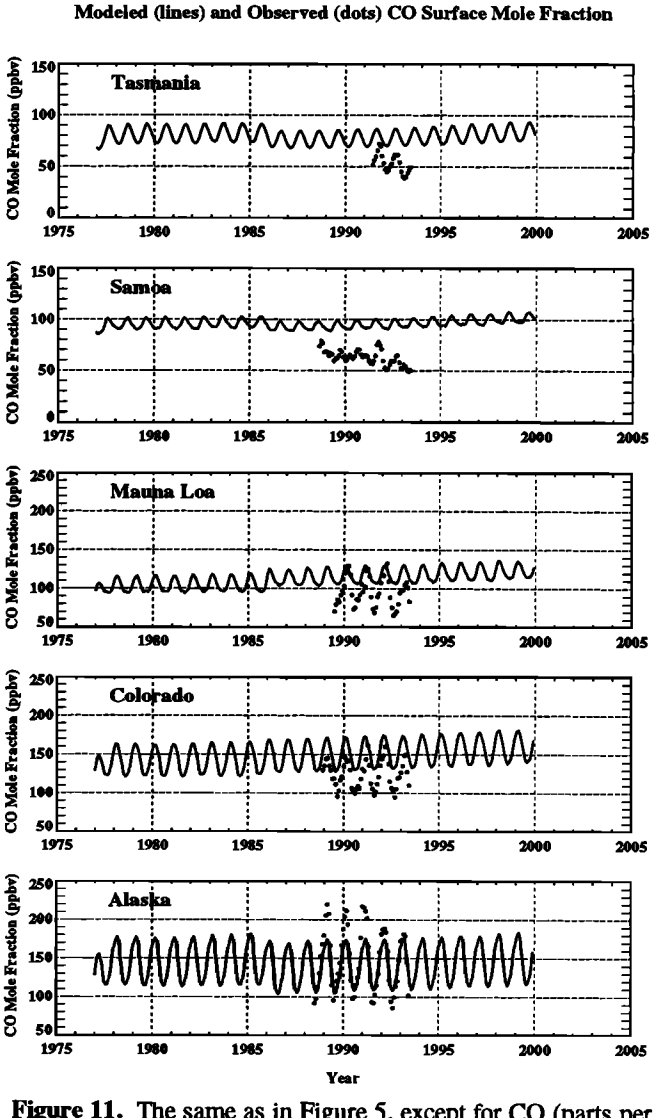

Figure 11. The same as in Figure 5, except for CO (parts per billion) at five NOAA/CMDL stations.

zonal averaging, oceanic dynamics and interaction with the atmosphere, the sulfate aerosol effect on the radiation, stratosphere-troposphere exchange (especially when related to ozone), and the effect of the neglected contributions of nonmethane hydrocarbons (many of them relate to polluted regions) on tropospheric chemistry. To narrow these uncertainties, further work is needed.

Acknowledgments. We thank Dana Hartley (GaTech) for providing chlorofluorocarbon emission data, the ALE/GAGE/AGAGE and NOAA/CMDL research teams for access to global trace gas measurement data, and Ed Hare (AES/Environment Canada) for providing WODC ozone data. Several MIT colleagues provided important input: Peter Stone helped with model transport development, especially the eddy diffusion part; Gary Holian played a major role in developing the oceanic carbon model; Jin Huang contributed to the CH_3CCl_3 simulations; Yuexin Liu developed the natural emission model; Jean Fitzmaurice provided help with emission calculations; and Zili Yang and Henry Jacoby and their colleagues provided EPPA model outputs for anthropogenic emissions. Advice regarding the land biospheric uptake of CO_2 was provided by Xiangming Xiao and David Kicklighter (Marine Biological Laboratory). This research is a part of the MIT Joint Program on the Science and Policy of Global Change, which is supported by a number of industrial sponsors: by Asea Brown Boveri (Switzerland), Atlantic Richfield Company (USA), American Automobile Manufacturers Association (Chrysler, Ford, General Motors), British Petroleum Company (UK), Chevron Corporation (USA), Cyprus Amax Coal Company (USA), Electric Power Research Institute (USA), Exxon Corporation (USA), Mobil Corporation (USA), Petrofina SA. (Belgium), RWA/Rheinbraun (Germany), Saudi Arabian Oil Company, Shell Internationale Petroleum (The Netherlands), Statoil (Norway), Texaco Incorporated (USA), The Tokyo Electric Power Company (Japan); by the U.S. Department of Energy (901214-HAR; DE-FG02-94ER61937; DE-FG02-93ER61713), U.S. National Science Foundation (9523616-ATM), U.S. National Oceanic and Atmospheric Administration (NA56GP0376), and U.S. Environmental Protection Agency (CR-820662-02); by the Royal Norwegian Ministries of Industry and Energy and Foreign Affairs; and by the G. Unger Vetlesen Foundation (USA).

References

Alternative Fluorocarbons Environmental Acceptability Study (AFEAS), Production, sales and atmospheric release of fluorocarbons through 1994, report, AFEAS Admin. Org., Washington, D. C., 1994.

Atkinson, P. S., D. L. Baulch, R. A. Cox, R. S. Hampson, Jr., J. A. Kerr, and J. Troe, Evaluated kinetic and photochemical data for atmospheric chemistry, *J. Phys. Chem. Ref. Data*, *21*(6), 1125-1444, 1992.

Bott, A., A positive definite advection scheme obtained by nonlinear renormalization of the advective fluxes, *Mon. Weather Rev.*, *117*, 1006-1015, 1989a.

Bott, A., Reply to Smolarkiewicz's comment, *Mon. Weather Rev.*, *117*, 2633-2636, 1989b.

Bott, A., The monotone area-preserving flux-form advection algorithm: Reducing the time-splitting error in two-dimensional flow fields, *Mon. Weather Rev.*, *121*, 2637-2641, 1993.

Chin, M., D. J. Jacob, G. M. Gardner, and D. L. Savoie, A global three-dimensional model of tropospheric sulfate, *J. Geophys. Res.*, *101*, 18,667-18,690, 1996.

Crutzen, P. J., and P. H. Zimmermann, The changing photochemistry of the troposphere, *Tellus*, *43AB*, 136-151, 1991.

Cunnold, D. M., P. J. Fraser, R. F. Weiss, R. G. Prinn, P. G. Simmonds, B. R. Miller, F. N. Alyea, and A. J. Crawford, Global trends and annual releases of CCl_3F and CCl_2F_2 estimated from ALE/GAGE and other measurements from July 1978 to June 1991, *J. Geophys. Res.*, *99*, 1107-1126, 1994.

DeMore, W. B., S. P. Sander, D. M. Golden, R. F. Hampson, M. J. Kurylo, C. J. Howard, A. R. Ravishankara, C. E. Kolb, and M. J. Molina, Chemical kinetics and photochemical data for use in stratospheric modeling: Evaluation number 11, *JPL Publ. Rep.* 94-26, 1994.

Derwent, R. G., The influence of human activities on the distribution of hydroxyl radicals in the troposphere, *Philos. Trans. R. Soc. London, Ser. A*, *354*, 501-531, 1996.

Ehhalt, D. H., F. Rohrer, and A. Wahner, Sources and distribution of NO_x in the upper troposphere at northern midlatitudes, *J. Geophys. Res.*, *97*, 3725-3738, 1992.

Fisher, D. A., T. Duafala, P. M. Midgley, and C. Niemi, Production and emission of CFCs, halons, and related Molecules: Report on concentrations, lifetimes, and trends of CFCs, halons, and related species, *NASA Ref. Publ. 1339*, 1994.

Fraser, P., M. Gunson, S. Penkett, F. S. Rowland, U. Schmidt, and R. Weiss, Measurements: Report on concentrations, lifetimes, and trends of CFCs, halons, and related species, *NASA Ref. Publ. 1339*, 1994.

Fung, I., J. John, J. Lerner, E. Matthews, M. Prather, L. P. Steele, and P. J. Fraser, Three-dimensional model synthesis of the global methane cycle, *J. Geophys. Res.*, *96*, 13,033-13,065, 1991.

Golombek, A., and R. G. Prinn, A global three-dimensional model of the circulation and chemistry of $CFCl_3$, CF_2Cl_2, CH_3CCl_3, CCl_4, and N_2O, *J. Geophys. Res.*, *91*, 3985-4001, 1986.

Golombek, A., and R. G. Prinn, A global three-dimensional model of the stratospheric sulfuric acid layer, *J. Atmos. Chem.*, *16*, 179-199, 1993.

Graedel, T. E., Global emission inventories to aid atmospheric modelers, *Eos Trans. AGU*, *75*(50), 585, 1994.

Hansen, J., G. Russel, D. Rind, P. H. Stone, A. Lacis, S. Lebedeff, R. Ruedy, and L. Travis, Efficient three-dimensional global models for climate studies: Model I and model II, *Mon. Weather Rev.*, *111*, 609-662, 1983.

Hartley, D., and R. G. Prinn, Feasibility of determining surface emissions of trace gases using an inverse method in a three-dimensional chemical transport model, *J. Geophys. Res.*, *98*, 5183-5198, 1993.

Hauglustaine, D. A., C. Granier, G. P. Brasseur, and G. Megie, The importance of atmospheric chemistry in the calculation of radiative forcing on the climate system, *J. Geophys. Res.*, *99*, 1173-1186, 1994.

Hindmarsh, A. C., ODEPACK, A systematized collection of ODE solvers, in *Scientific Computing*, edited by R. S. Stepleman et al., pp. 55-64, North-Holland, New York, 1983.

Hough, A. M., Development of a two-dimensional global tropospheric model: Model chemistry, *J. Geophys. Res.*, *96*, 7325-7362, 1991.

International Panel on Climate Change, *Climate Change 1994: Radiative Forcing of Climate Change and an Evaluation of the IPCC IS92 Emission Scenarios*, 339 pp., Cambridge Univ. Press, New York, 1994.

International Panel on Climate Change, *Climate Change 1995: The Science of Global Change*, 572 pp., Cambridge Univ. Press, New York, 1996.

Jaffe, D. A., T. K. Berntsen, and S. A. Isaksen, A global three-dimensional chemical transport model, 2, Nitrogen oxides and nonmethane hydrocarbon results, *J. Geophys. Res.*, *102*, 21,281-21,296, 1997.

Kanakidou, M., H. B. Singh, K.M. Valentin, and P.J. Crutzen, A two-dimensional study of ethane and propane oxidation in the troposphere, *J. Geophys. Res.*, *96*, 15,395-15,413, 1991.

Kitada, T., Effect of non-zero divergence wind fields on atmospheric transport calculations, *Atmos. Environ.*, *21*, 785-788, 1987.

Kumar, P. P., G. K. Manohar, and S. S. Kandalgaonkar, Global distribution of nitric oxide produced by lightning and its seasonal variation, *J. Geophys. Res.*, *100*, 11,203-11,208, 1995.

Law, K. S., and J. A. Pyle, Modeling trace gas budgets in the troposphere, 1, Ozone and odd nitrogen, *J. Geophys. Res.*, *98*, 18,377-18,400, 1993.

Levy, H., II, W. J. Moxim, and P. S. Kasibhatla, A global three-dimensional time-dependent lightning source of tropospheric NO_x, *J. Geophys. Res.*, *101*, 22,911-22,922, 1996.

Levy, H., II, P. S. Kasibhatla, W. J. Moxim, A. A. Klonecki, A. I. Hirsch, S. J. Oltmans, and W. L. Chameides, The human impact on global tropospheric ozone, *Geophys. Res. Lett.*, *24*(7), 791-794, 1997.

Liu, Y., Modeling the emissions of nitrous oxide (N_2O) and methane

(CH_4) from the terrestrial biosphere to the atmosphere, *Rep. 10*, 219 pp., Mass. Inst. of Technol. Joint Program on the Sci. and Policy of Global Change, Cambridge, 1996.

Logan, J. A., Trends in the vertical distribution of ozone: An analysis of ozonesonde data, *J. Geophys. Res.*, *99*, 25,553-25,585, 1994.

Moxim, W. J., H. Levy II, and P. S. Kasibhatla, Simulated global tropospheric PAN: Its transport and impact on NO_x, *J. Geophys. Res.*, *101*, 12621-12638, 1996.

Novelli, P. C., L. P. Steele, and P. P. Tans, Mixing ratio of carbon monoxide in the troposphere, *J. Geophys. Res.*, *97*, 20,731-20,750, 1992.

Orr, J. C., Accord between ocean models predicting uptake for anthropogenic CO_2, *Water Air and Soil Pollut.*, *70*, 465-481, 1993.

Pandis, S. N., and J. H. Seinfeld, Sensitivity analysis of chemical mechanism for aqueous-phase atmospheric chemistry, *J. Geophys. Res.*, *94*, 1105-1126, 1989.

Prinn, R. G., Toward an improved global network for determination of tropospheric ozone climatology and trends, *J. Atmos. Chem.*, *6*, 281-298, 1988.

Prinn, R. G., D. Cunnold, R. Rasmussen, P. Simmonds, F. Alyea, A. Crawford, P. Fraser, and R. Rosen, Atmospheric emissions and trends of nitrous oxide deduced from 10 years of ALE-GAGE data, *J. Geophys. Res.*, *95*, 18,369-18,385, 1990.

Prinn, R. G., R. F. Weiss, B. R. Miller, J. Huang, F. N. Alyea, D. M. Cunnold, P. J. Fraser, D. E. Hartley, and P. G. Simmonds, Atmospheric trends and lifetime of CH_3CCl_3 and global OH concentrations, *Science*, *269*, 187-192, 1995.

Prinn, R. G., et al., Integrated global system model for climate policy assessment: Feedbacks and sensitivity studies, *Clim. Change*, in press, 1997.

Roelofs, G.-J., and J. Lelieveld, Distribution and budget of O_3 in the troposphere calculated with a chemistry general circulation model, *J. Geophys. Res.*, *100*, 20,983-20,998, 1995.

Sarmiento, J. L., J. C. Orr, and U. Siegenthaler, A perturbation simulation of CO_2 uptake in an ocean general circulation model, *J. Geophys. Res.*, *97*, 3621-3645, 1992.

Seinfeld, J. H., *Atmospheric Chemistry and Physics of Air Pollution*, John Wiley, New York, 1986.

Singh, H. B., et al., Reactive nitrogen and ozone over the western Pacific: Distribution, partitioning, and sources, *J. Geophys. Res.*, *101*, 1793-1808, 1996.

Smolarkiewicz, P. K., and W. W. Grabowski, The multidimensional positive definite advection transport algorithm: Nonoscillatory option, *J. Comput. Phys.*, *86*, 355-375, 1990.

Sokolov, A. P., and P. H. Stone, Description and validation of the MIT version of the GISS 2D Model, *Rep. 2*, 46 pp., Mass. Inst. of Technol. Joint Program on the Sci. and Policy of Global Change, Cambridge, 1995.

Sokolov, A. P., and P. H. Stone, A flexible climate model for use in integrated assessments, *Rep. 17*, 16 pp., Mass. Inst. of Technol. Joint Program on the Sci. and Policy of Global Change, Cambridge, 1997.

Spiro, P. A., D. J. Jacob, and J. A. Logan, Global inventory of sulfur emissions with 1° × 1° resolution, *J. Geophys. Res.*, *97*, 6023-6036, 1992.

Stockwell, W. R., On the $HO_2 + HO_2$ reaction: Its misapplication in atmospheric chemistry models, *J. Geophys. Res.*, *100*, 11,695-11,698, 1995.

Stone, P. H., and M. S. Yao, Development of a two-dimensional zonally averaged statistical-dynamical model, II, The role of eddy momentum fluxes in the general circulation and their parameterization, *J. Atmos. Sci.*, *44*, 3769-3786, 1987.

Stone, P. H., and M. S. Yao, Development of a two-dimensional zonally averaged statistical-dynamical model, III, The parameterization of the eddy fluxes of heat and moisture, *J. Clim.*, *3*, 726-740, 1990.

Taylor, K. E., and J. E. Penner, Response of the climate system to atmospheric aerosols and greenhouse gases, *Nature*, *369*, 734-737, 1994.

Wang, C., and J. S. Chang, A three-dimensional numerical model of cloud dynamics, microphysics, and chemistry, 1, Concepts and formulation, *J. Geophys. Res.*, *98*, 14,827-14,844, 1993.

Wang, C., and P. J. Crutzen, Impact of a simulated severe local storm on the redistribution of sulfur dioxide, *J. Geophys. Res.*, *100*, 11,357-11,367, 1995.

Xiao, X., D. W. Kicklighter, J. M. Melillo, A. D. McGuire, P. H. Stone, and A. Sokolov, Linking a global terrestrial biogeochemical model and a 2-dimensional climate model: Implications for the global carbon budget, *Tellus, Ser. B*, *49*, 18-27, 1997.

Yang, Z., R. S. Eckaus, A. D. Ellerman, and H. D. Jacoby, The MIT Emissions Prediction and Policy Analysis (EPPA) Model, *Rep. 6*, 49 pp., Mass. Inst. of Technol. Joint Program on the Sci. and Policy of Global Change, Cambridge, 1996.

Yao, M. S., and P. H. Stone, Development of a two-dimensional zonally averaged statistical-dynamical model, I, The parameterization of moist convection and its role in the general circulation, *J. Atmos. Sci.*, *44*, 65-82, 1987.

R. G. Prinn, A. Sokolov, and C. Wang, Joint Program on the Science and Policy of Global Change, Massachusetts Institute of Technology, 77 Massachusetts Avenue, Building E40-269, Cambridge, MA 02139-4307. (e-mail: wangc@mit.edu)

(Received August 11, 1997; revised October 17, 1997;
accepted November 26, 1997.)